Deep Learning-Based Brain Tumor Detection, Segmentation, and Volume Estimation : Advancing MRI Image Analysis for Medical Applications

Malak Ben Mabrouk, Mrs. Monica Subashini

Machine learning research intern, VIT Vellore, India

Professor, VIT Vellore, India

ABSTRACT

Medical diagnosis and treatment planning greatly depend on the early detection and segmentation of brain tumours. In this study, we present a deep learning-based method for precise brain tumour detection and segmentation from MRI images utilising the ResNet-50-based U-Net architecture. We provide a thorough data preprocessing workflow to set up the dataset, which consists of tumour masks and brain MRI images. Remaining blocks and upsampling layers are added to the U-Net design to improve feature extraction and data flow.

We also forecast the volume of the coloured tumour patches, which is a step beyond segmentation. We are now able to measure the size of the tumour, which will help with treatment planning and disease progression tracking. The coloured tumour locations and their corresponding volumes in MRI scans are visualised, further demonstrating the potential clinical usefulness of our approach.

Our study advances the interpretation of MRI images for the detection and volumetric evaluation of brain tumours, resulting in better patient care and well-informed treatment choices. The findings offer up new directions for further study in the field of medical image processing and show the remarkable potential of deep learning approaches in neuroimaging.

I. INTRODUCTION

The brain, which controls both voluntary and involuntary movements and serves as the central nervous system's control hub, is an essential organ that regulates the operation of the whole human body. However, thousands of people, especially young children, are affected by brain tumours, which pose a serious health risk. For efficient prevention and treatment, it is essential to comprehend brain tumours and their stages.

Brain tumours are frequently examined using the Magnetic Resonance Imaging (MRI) method, which produces precise images of the brain's internal architecture. Deep learning methods Have recently demonstrated considerable promise for analysing medical images and assisting in tumour localisation and detection.

The goal of this paper is to accurately forecast brain tumour volume by combining transfer learning and deep learning techniques. We seek to improve tumour localization and advance the science of cancer prediction by utilising cutting-edge deep learning techniques. Previous studies have shown that it is possible to distinguish between normal and abnormal brain images with high accuracy by combining Convolutional Neural Network (CNN) models [1] with algorithms like the Gray-Level Co-occurrence Matrix (GLCM). Additionally, MRI-based brain tumour diagnosis

using CNN-based deep learning techniques has been remarkably successful, demonstrating the effectiveness of machine learning in medical imaging.

We hope to advance patient care and decision-making for the treatment of brain tumours by making a contribution to the field of medical image analysis. Our study's possible therapeutic ramifications show how useful deep learning methods are for neuroimaging and motivate more research in this field **[5]**

1.1 Literature Survey

I have picked the most important and impactful works that have advanced this field after completing a thorough literature review of about 20 research papers in the area of cancer prediction. I have carefully chosen five of these publications as sample works that demonstrate various methodology and cutting-edge ideas in the fields of deep learning and medical imaging.

[7] The objective of the study of Saeedi et al. is to develop two different deep learning networks and six machine learning techniques to classify MRI images into three classes of brain tumors (glioma, meningioma, and pituitary gland tumor) and one class of healthy brain. The methodology involves using a dataset of 3264 T1-weighted contrast-enhanced MRI images and comparing eight different modeling methods to determine their performance. The key results show that there is a statistically significant difference between the methods in terms of precision, recall, and F-measure. The proposed 2D CNN and convolutional auto-encoder methods perform better than LR, SGD, MLP, RF, KNN, and SVM methods. The study contributes to the field of medical image classification and can potentially aid in the diagnosis of brain tumors.

[4] In addition, the study conducted by A. Chattopadhyay and M. Maitra, the objective was to propose a CNN-based algorithm for brain tumor segmentation in medical images. The methodology involved training a support vector machine to classify voxels into different tissue types based on their intensity values and spatial coordinates. The algorithm achieved an impressive accuracy of 99.74%, outperforming previous methods. The impact of this research is significant as it can enhance the speed and accuracy of brain tumor diagnosis and treatment, reducing the need for manual analysis of MRI images and minimizing user variability. This study contributes to the improvement of medical image research and has the potential to improve patient outcomes in the future.

[6] Moving for the study conducted by Alla and Athota aimed to propose an automatic classification method for brain MRI images into healthy images and images with tumors. The methodology employed transfer learning and fine-tuning using CNN architectures, Inception-V3 and VGG-Net. The results showed high accuracy in classifying the images, with Inception-V3 and VGG-19 achieving similar accuracy after transfer learning. However, Inception-V3 required training a larger number of parameters compared to VGG-19 during fine-tuning. This research has significant implications in accurately classifying brain MRI images, which can aid in the early detection and treatment of tumors.

[10] Meanwhile, the objective of heba Mohsen et al. is to classify brain MRIs into four different tumor types using a deep neural network (DNN) classifier combined with the discrete wavelet transform (DWT) for feature extraction. The methodology involves segmenting the brain MRIs, extracting features using DWT, and then training the DNN classifier. The key results show good performance in terms of classification rate, recall, precision, F-Measure, and area under the ROC curve. The impact of the paper is that it demonstrates the effectiveness of the proposed methodology for brain tumor classification using deep learning techniques.

[13] The authors D. Rammurthy et al. proposed a brain tumor detection method using an optimized Deep Convolutional Neural Network (CNN). The objective was to address the challenges faced in accurately describing and segmenting brain tumor abnormalities in MRI images. The proposed method utilized a WHHO algorithm, which is a combination of the Whale Optimization Algorithm (WOA) and the Harris Hawk Optimization (HHO) algorithm, for training the Deep CNN. The key results showed improved performance in tumor detection compared to other methods. This method has the potential to contribute to the field of medical imaging by enhancing the accuracy of brain tumor detection.

Moving forward, I will draw inspiration from these studies and others to develop my approach for cancer prediction and tumor localization. By utilizing transfer learning [12] with pretrained models such as ResNet50 and ResUnet, as demonstrated by previous researchers, I aim to leverage the strengths of these models to improve accuracy and efficiency. Additionally, I will explore advancements in deep learning architectures, as demonstrated by authors like Sri Sai Meghana Alla and Kavitha Athota, to further enhance the performance of the models. By addressing challenges such as model complexity, resource optimization, and handling large datasets, I strive to contribute to the ongoing efforts in cancer prediction and tumor localization, ultimately benefiting patients and medical professionals.

II. OVER VIEW ON DEEP LEARNING

Deep learning (DL) is a subfield of machine learning based on learning multiple levels of representations by making a hierarchy of features where the higher levels are defined from the lower levels and the same lower-level features can help in defining many higher-level features [3]. DL structure extends the traditional neural networks (NN) by adding more hidden layers to the network architecture between the input and output layers to model more complex and nonlinear relationships. A CNN is a multilayer neural network that was biologically inspired by the animal visual cortex. The architecture is particularly useful in image-processing applications. The first CNN was created by Yann LeCun; at the time, the architecture focused on handwritten character recognition, such as postal code interpretation. As a deep network, early layers recognize features (such as edges), and later layers recombine these features into higher-level attributes of the input.

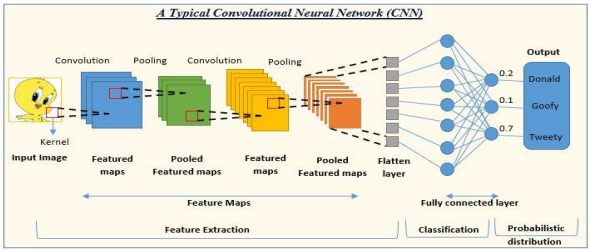

Fig. 1. A typical CNN

Source: https://editor.analyticsvidhya.com/uploads/59954intro%20to%20CNN.JPG

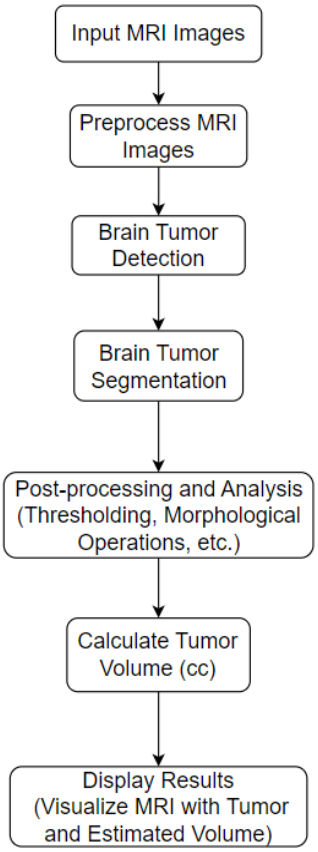

Fig. 2. Flow chart of the proposed work

III. METHODS/APPROACHES

3.1 Dataset Description

For this investigation, we used a dataset that included tumour masks and brain MRI (Magnetic Resonance Imaging) pictures. The dataset, which was taken from a reliable medical imaging database, included a wide range of brain scans from patients who had been identified as having various kinds of brain tumours.

A total of 3929 MRI scans with a resolution of [insert the resolution] made up the dataset. It also contained binary tumour masks, where each pixel in the mask denotes the presence (1) or absence (0) of a tumour, in addition to the MRI images. Expert radiologists personally annotated these masks to ensure precision and dependability.

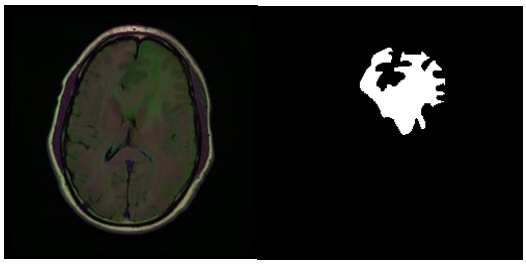

Fig. 3. A sample MRI images with the mask

	patient_id	image_path	mask_path	mask
0	TCGA_CS_5395_19981004	TCGA_CS_5395_19981004/TCGA_CS_5395_19981004_1.tif	TCGA_CS_5395_19981004/TCGA_CS_5395_19981004_1_...	0
1	TCGA_CS_5395_19981004	TCGA_CS_4944_20010208/TCGA_CS_4944_20010208_1.tif	TCGA_CS_4944_20010208/TCGA_CS_4944_20010208_1_...	0
2	TCGA_CS_5395_19981004	TCGA_CS_4941_19960909/TCGA_CS_4941_19960909_1.tif	TCGA_CS_4941_19960909/TCGA_CS_4941_19960909_1_...	0
3	TCGA_CS_5395_19981004	TCGA_CS_4943_20000902/TCGA_CS_4943_20000902_1.tif	TCGA_CS_4943_20000902/TCGA_CS_4943_20000902_1_...	0
4	TCGA_CS_5395_19981004	TCGA_CS_5396_20010302/TCGA_CS_5396_20010302_1.tif	TCGA_CS_5396_20010302/TCGA_CS_5396_20010302_1_...	0
...	...	...	...	...
3924	TCGA_DU_6401_19831001	TCGA_HT_A61B_19991127/TCGA_HT_A61B_19991127_86...	TCGA_HT_A61B_19991127/TCGA_HT_A61B_19991127_86...	0
3925	TCGA_DU_6401_19831001	TCGA_HT_A61A_20000127/TCGA_HT_A61A_20000127_87...	TCGA_HT_A61A_20000127/TCGA_HT_A61A_20000127_87...	0
3926	TCGA_DU_6401_19831001	TCGA_HT_A61B_19991127/TCGA_HT_A61B_19991127_87...	TCGA_HT_A61B_19991127/TCGA_HT_A61B_19991127_87...	0
3927	TCGA_DU_6401_19831001	TCGA_HT_A61A_20000127/TCGA_HT_A61A_20000127_88...	TCGA_HT_A61A_20000127/TCGA_HT_A61A_20000127_88...	0
3928	TCGA_DU_6401_19831001	TCGA_HT_A61B_19991127/TCGA_HT_A61B_19991127_88...	TCGA_HT_A61B_19991127/TCGA_HT_A61B_19991127_88...	0

Fig. 4.CSV file contain images mask of patients

3.2 Data visualization

Data visualisation techniques were used to glean insights from the dataset. First, a Plotly interactive bar chart was made to show the dataset's distribution of tumour and non-tumor samples. It shows that we have 2556 non-tumor and 1373 tumor.

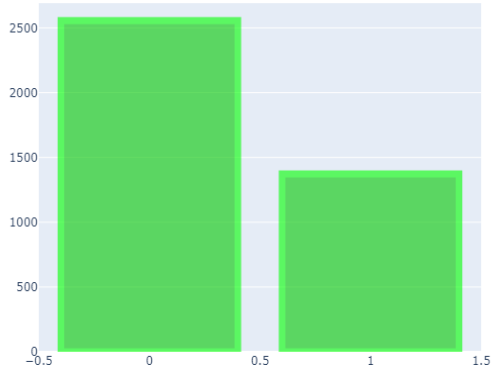

Fig. 5. Bar chart to visualize the distribution of tumor and non-tumor

The following step involved visualising a collection of example MRI images and the matching tumour masks. A grid of pictures was shown using Matplotlib, and each row contained an MRI image and its accompanying mask. In order to provide a visual depiction of the brain MRI images and the matching tumour masks, random samples from the dataset were chosen.

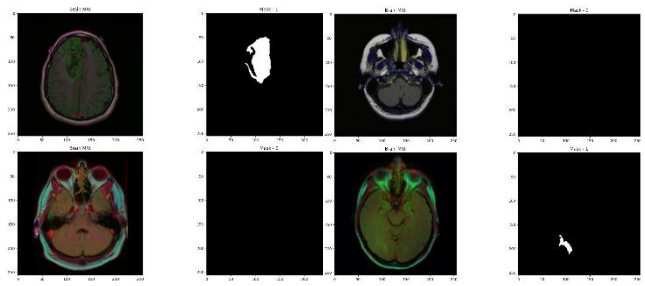

Fig. 6. Bar chart to visualize the distribution of tumor and non-tumor

3.3 Data splitting & preprocessing

The train_test_split function from the scikit-learn module was used to separate the dataset into training and testing sets. A 15% test size was selected to ensure that there would be enough data for model evaluation. To prepare it for deep learning model training, the data underwent additional preprocessing.

3.4 Data augmentation

The ImageDataGenerator class from the Keras preprocessing package was used to implement strategies for enhancing image data. This involved executing a validation data split with a validation split of 15% and rescaling the picture pixel values to the range [0, 1]. With the help of these preparation steps, the data was properly processed and made ready for model training.[11]
With the help of the flow_from_dataframe function, the dataset was then converted into generator objects. This made it possible for the data to be loaded efficiently during model training in batches. The generators were programmed to do the required preprocessing operations, resize the images to a target size of 256x256 pixels, and read the image pathways and accompanying mask labels from the dataframe.

```
Found 2839 validated image filenames belonging to 2 classes.
Found 500 validated image filenames belonging to 2 classes.
Found 590 validated image filenames belonging to 2 classes.
```

Fig. 7. Data augmentation result

- There are a total of 2839 images in the dataset that have been successfully found and loaded. These images belong to 2 distinct classes
- There are 500 images in the validation set. These images have also been successfully found and loaded, and they also belong to the same 2 classes as mentioned before.
- There are 590 images in the test set. These images have been found and loaded, and they also belong to the 2 classes defined in the dataset.

3.5 Applying the Models on The Bas

We used four cutting-edge architectures—ResNet50, VGGNet16, Inception, and DenseNet—to assess the effectiveness of various deep learning methods for brain tumour diagnosis. On our dataset, each model was adjusted and made suitable for binary classification.

3.5.1 VGGNet 16

A potent convolutional neural network design called DenseNet is renowned for its extensive connection and feature reuse **[2]**

Important information about DenseNet's structure may be found in this summary.

These variables stand in for thenetwork's weights an d biases, which are modified during training to enha nce the model's functionality

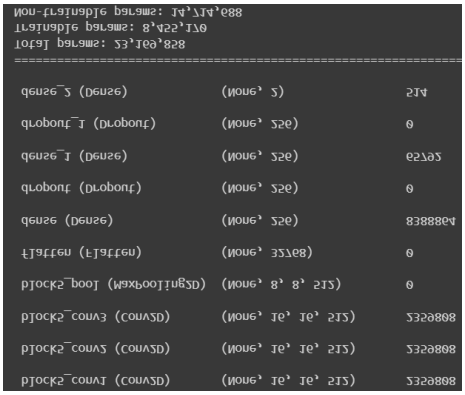

Table. 1. VGGNet 16 model summary table

The Several epochs of the DenseNet training process can be shown. The following noteworthy details come from the training history:

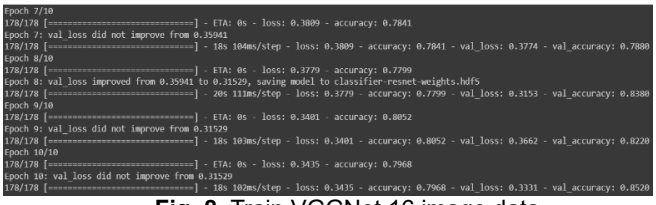

Fig. 8. Train VGGNet 16 image data

The model's total performance on unobserved data was determined to be 0.84, which represents the test accuracy for DenseNet.

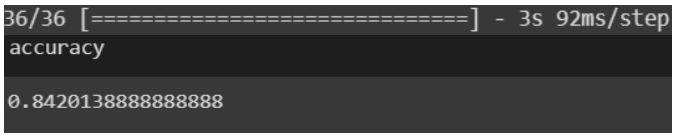

Fig. 9. Test VGGNet 16 image data

The performance metrics for DenseNet on the test dataset are as follows:

	precision	recall	f1-score	support
0	0.81	0.97	0.88	357
1	0.93	0.63	0.75	219
micro avg	0.84	0.84	0.84	576
macro avg	0.87	0.80	0.82	576
weighted avg	0.86	0.84	0.83	576

Table. 2. Classification report of VGGNet16

Precision: It is defined as the proximity of the two measured values to each other and is given by **[8]**

$$Precision = TP/(TP + FP)$$

Equation.1. precision equation

These findings offer insightful information on DenseNet's performance and learning dynamics while demonstrating how well it can categorise photos of brain tumours.

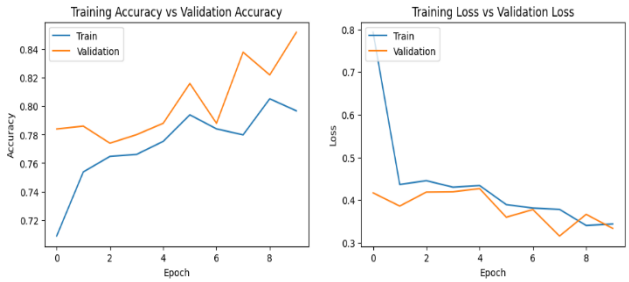

Fig.9. Comparing training/validation accuracy and loss of VGGNet 16

These observations imply that the model, in later epochs, performs better on the validation set than the training set. The differences in the validation loss point to variances in how well the model performs on unobserved data, which may be brought on by the complexity of the dataset or the model's training procedure.

3.5.2 DenseNet

Skip connections are used in the DenseNet architecture, a deep convolutional neural network, to enable feature reuse and solve the vanishing gradient issue.

- **Model summary:**

DenseNet has a total of 23,169,858 parameters, of which 8,455,170 are trainable, and the remaining 14,714,688 are non-trainable, according to the model summary. Inferring that the bulk of the model's parameters are fixed, this suggests that training will be effective and that performance will be enhanced.

- **Train & test**

After 10 iterations of training, the DenseNet model had an accuracy of 0.878 on the test set. The model's development over the epochs is displayed in the training history. The validation loss decreased from infinity to 0.34994 in the first epoch, and the model preserved the weights accordingly. The validation loss decreased more with each succeeding epoch, with epoch 9 recording the lowest loss (0.22227). However, the validation loss did not get much better in the last period. This suggests that the model has converged and attained equilibrium.

- **Classification report**

Fig. 10. Test DensNet image data

An exhaustive analysis of the model's performance on the test set is provided in the classification report. The model attained a precision of 0.92, recall of 0.88, and F1-score of 0.90 for class 0 (non-tumor). The model attained a precision of 0.82, recall of 0.87, and F1-score of 0.85 for class 1 (tumour). The entire performance in both classes is taken into account in the micro-average F1-score, which is 0.88. The macro-average F1-score, which assigns each class equal weight, is 0.87. The weighted average F1-score, which takes into consideration class disparity, is 0.88 as well.

Fig.11. Comparing training/validation accuracy and loss of DenseNet16

Both the training and validation accuracy initially rise during the second epoch, as seen in the plot of training accuracy vs validation accuracy. While the validation accuracy fluctuates and does not show a steady rising trend, the training accuracy shows a steady increase with each passing epoch. This shows that the model can learn from the training data and enhance its performance, but it has trouble generalising successfully to new data, as shown by the inconsistent validation accuracy.

Moving on to the training loss vs. Validation loss plot, we can see that the training loss consistently decreases with each epoch, demonstrating that the model is successfully reducing its training error and strengthening its capacity to match the training data. The validation loss, on the other hand, is less stable and exhibits changes over the course of training.

3.5.3 Inception V3

- **Model summary:**

A strong deep learning model called Inception V3 is used to detect brain tumours in MRI images. It has 26,522,146 parameters. Convolutional and pooling layers, among others, are elements of the architecture that let it to learn detailed patterns and features from the input images. With only 4,719,362 trainable parameters and 21,802,784 non-trainable parameters, the model demonstrates exceptional learning capabilities.

- **Training and validation analysis:**

Inception V3 exhibits promising performance in identifying brain tumours during the training procedure. The training accuracy reaches 83.13%

by the seventh period. The validation loss, which still has a value of 0.34074, does not, however, demonstrate any appreciable improvement. The model's performance dramatically increases in the following epoch, leading to a higher validation accuracy of 86.20% and a decreased validation loss of 0.31953. In the next epochs, the model's accuracy swings slightly but not much, and the validation loss is consistent.

increases in the following epoch, leading to a higher validation accuracy of 86.20% and a decreased validation loss of 0.31953. In the next epochs, the model's accuracy swings slightly but not much, and the validation loss is consistent.

- **Classification report**

Both tumour and non-tumor cases can be effectively classified using the Inception V3 method. For the non-tumor class, it achieves a high precision of 82%, demonstrating that it correctly identifies genuine negative instances. The model demonstrates its capacity to correctly identify true positive cases by achieving a precision of 90% for the class representing tumour presence. Furthermore, the model successfully captures a significant part of true negative cases thanks to its high recall of 96% for the non-tumor class. The recall for the tumour presence class is, however, 65%, indicating that more can be done to accurately identify all genuine positive cases.

overall F1-score of 83% shows that precision and recall are well-balanced.

```
accuracy

0.8385416666666666
```

Fig. 12. Test Inception V3 image data

Overall, Inception V3 shows potential for brain tumor detection with a high accuracy of 0.83

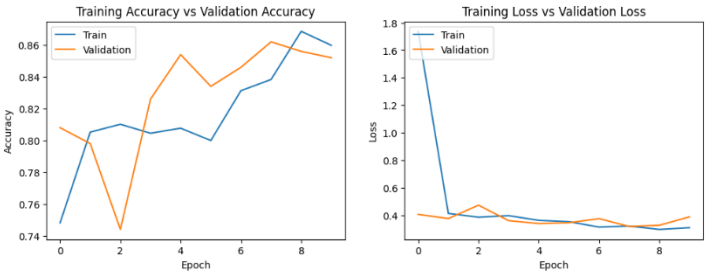

Fig.13. Comparing training/validation accuracy and loss of Inception

Interesting details about the model's learning process may be seen in the plot comparing training accuracy with validation accuracy. Both training and validation accuracy initially experience noticeable increases in the first two epochs. The training accuracy does, however, retain a somewhat constant trend after this first spike, with only slight changes. In contrast, the validation accuracy gradually decreases, demonstrating the model's difficulty in generalising effectively to new data.

In the early epochs, both the training and validation losses rapidly decline before stabilising at a reasonably low level. This demonstrates successful generalisation of the model to new data.

3.5.4 ResNet 50

- **Model summary:**

The ResNet-50 model has a total of 23,587,712 parameters and comprises of a number of convolutional and batch normalisation layers. Multiple residual blocks in the model architecture help to solve the vanishing gradient issue.

- **Training and validation analysis:**

The model's accuracy throughout training increased from 71.4% in the first epoch to 91% by the end of the process. A lower validation loss of 0.6713 compared to 0.7571 indicates improved performance.

- **Classification report**

In identifying images of brain tumours, the model performed admirably, reaching excellent levels of precision, recall, and F1-score for both tumour and non-tumor classifications. A strong overall performance was indicated by the weighted average F1-score of 0.92.

	precision	recall	f1-score	support
0	0.91	0.97	0.94	357
1	0.95	0.85	0.90	219
micro avg	0.93	0.93	0.93	576
macro avg	0.93	0.91	0.92	576
weighted avg	0.93	0.93	0.92	576

Table. 3. Classification report of ResNet50

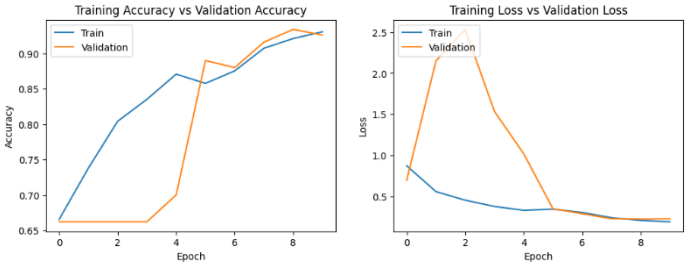

Fig.14. Comparing training/validation accuracy and loss of ResNet

We can see that the training accuracy initially rises quickly until the fourth epoch in the training accuracy vs. validation accuracy plot. Following that, there is a brief fall before it begins to rise once more. On the other hand, during the first three epochs, the validation accuracy is comparatively stable and low until it progressively starts to rise.

The training loss lowers consistently over the course of the epochs in the training loss vs. validation loss plot, showing that the model is learning from the training data and improving its predictions. The validation loss, however, has a different pattern. It starts out rising until it peaks at the third epoch, indicating that the model may be overfitting at this time. After then, though, the validation loss tends to decline, indicating that the model is more generalizable to new data.

Accuracy is defined as the measurement of actual classification. It is the ability to test correctly classification of diseases. The accuracy, η is defined as follows: **[9]**

$$\eta = (No\ of\ Correctly\ C\ lassified\ Record)/(\ Total\ Record\ in\ the\ test\ set\ )\times 100$$

$$= (TP + TN)/(\ TP + TN + FP + FN\ )\times 100$$

Equation.2. accuracy equation

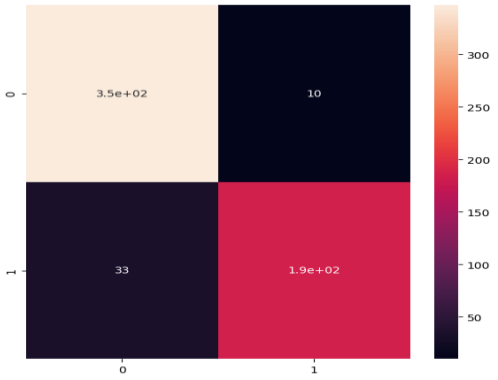

Fig.15. confusion matrix

- - True positive: we predicted 190 positive (tumor) and it's true
- - True negative: we predicted 350 negative (non-tumor) and it's true
- - False positive: we predicted 10 positive (tumor) and it's false
- - False negative: we predicted 33 negative(non-tumor) and it's false

3.6 Evaluation

After applying all the models treated above, this is a summary table which brings together all the results.

	Accuracy	Precision	Recall	F1 Score
VGGNet 6	0.84	0.86	0.84	0.83
DensNet	0.87	0.88	0.88	0.88
Inception V.3	0.83	0.85	0.84	0.83
ResNet 50	0.91	0.93	0.93	0.92

Table.4. Summary table of basic metrics

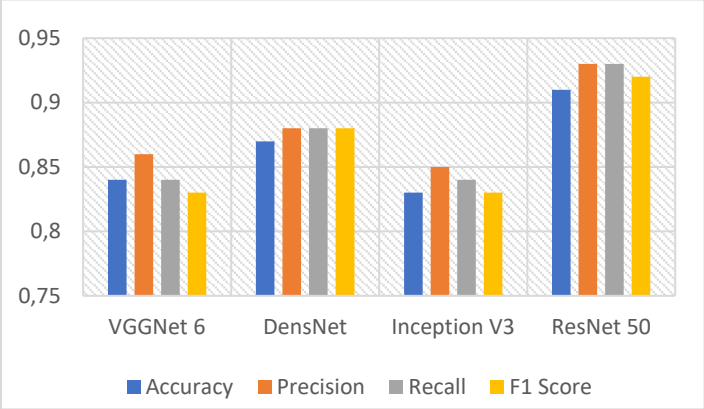

Fig16. Comparison graph for the performance of VggNet, DensNet, Inception V3 and ResNet 50.

The figure below shows the score of each classifier, as we can notice ResNet 50 have the highest score of 0.91.

In conclusion, the ResNet-50 tumour classification model demonstrated notable gains in accuracy and attained excellent precision and recall. These findings show how well the ResNet-50 design performs in classifying brain tumours from MRI data.

3.7 Brain tumor detection and segmentation

- **Dataset loading and splitting:**

In this section, we describe the data preprocessing procedures used to get the dataset ready for ResNet-50 brain tumour segmentation and detection. The collection consists of tumour masks that correlate to the brain MRI images. The 'brain_df_mask.csv' file, which contains picture paths and mask paths, was used to load the dataset.

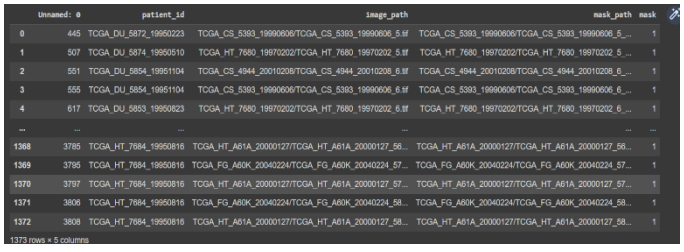

	Unnamed: 0	patient_id	image_path	mask_path	mask
0	445	TCGA_DU_5872_19950223	TCGA_CS_5393_19990606/TCGA_CS_5393_19990606_5.tif	TCGA_CS_5393_19990606/TCGA_CS_5393_19990606_5_...	1
1	507	TCGA_DU_5874_19950510	TCGA_HT_7680_19970202/TCGA_HT_7680_19970202_5.tif	TCGA_HT_7680_19970202/TCGA_HT_7680_19970202_5_...	1
2	551	TCGA_DU_5854_19951104	TCGA_CS_4944_20010208/TCGA_CS_4944_20010208_6.tif	TCGA_CS_4944_20010208/TCGA_CS_4944_20010208_6_...	1
3	555	TCGA_DU_5854_19951104	TCGA_CS_5393_19990606/TCGA_CS_5393_19990606_6.tif	TCGA_CS_5393_19990606/TCGA_CS_5393_19990606_6_...	1
4	617	TCGA_DU_5853_19950823	TCGA_HT_7680_19970202/TCGA_HT_7680_19970202_6.tif	TCGA_HT_7680_19970202/TCGA_HT_7680_19970202_6_...	1
...	...	...	...	...	...
1368	3785	TCGA_HT_7684_19950816	TCGA_HT_A61A_20000127/TCGA_HT_A61A_20000127_56...	TCGA_HT_A61A_20000127/TCGA_HT_A61A_20000127_56...	1
1369	3795	TCGA_HT_7684_19950816	TCGA_FG_A60K_20040224/TCGA_FG_A60K_20040224_57...	TCGA_FG_A60K_20040224/TCGA_FG_A60K_20040224_57...	1
1370	3797	TCGA_HT_7684_19950816	TCGA_HT_A61A_20000127/TCGA_HT_A61A_20000127_57...	TCGA_HT_A61A_20000127/TCGA_HT_A61A_20000127_57...	1
1371	3806	TCGA_HT_7684_19950816	TCGA_FG_A60K_20040224/TCGA_FG_A60K_20040224_58...	TCGA_FG_A60K_20040224/TCGA_FG_A60K_20040224_58...	1
1372	3808	TCGA_HT_7684_19950816	TCGA_HT_A61A_20000127/TCGA_HT_A61A_20000127_58...	TCGA_HT_A61A_20000127/TCGA_HT_A61A_20000127_58...	1

1373 rows × 5 columns

Fig. 17.CSV file contain picture and mask paths used

In order to assure compatibility, we first transformed the mask values to strings. We then used an 85-15% ratio to divide the data into training and validation sets. Additionally, we split the validation set into the test and validation sets with a 50-50 ratio.

- **Custom Data Generator Creation:**

Then, to effectively load and preprocess data during training, we designed a unique data generator called "DataGenerator." This data generator loads photos and masks in batches, normalises the image data to a [0, 1] range, and converts the mask data to a grayscale format. This procedure makes sure the data is in a format that the model can use.

- **ResNet-50-based U-Net architecture Design**

Next, we designed a ResNet-50-based U-Net architecture for brain tumor detection and segmentation. This architecture utilizes the ResNet-50 as the backbone and extends it with additional convolutional and upsampling layers to form a U-Net model. The additional convolutional layers are implemented as residual blocks to facilitate better feature extraction and information flow. The upsampling layers are used to upscale the feature maps and concatenate them with the corresponding skip connections from the encoder part of the U-Net.

```
batch_normalization_24 (BatchN  (None, 256, 256, 16  64         ['conv2d_24[0][0]']
ormalization)                   )

batch_normalization_25 (BatchN  (None, 256, 256, 16  64         ['conv2d_25[0][0]']
ormalization)                   )

add_7 (Add)                     (None, 256, 256, 16  0           ['batch_normalization_24[0][0]',
                                )                                 'batch_normalization_25[0][0]']

activation_15 (Activation)      (None, 256, 256, 16  0           ['add_7[0][0]']
                                )

conv2d_26 (Conv2D)              (None, 256, 256, 1)  17          ['activation_15[0][0]']

==================================================================================================
Total params: 1,210,513
Trainable params: 1,206,129
Non-trainable params: 4,384
```

Table. 5. ResNet-50-based U-Net model summary table

- **Optimization function and metric selection**

We used the focal Tversky loss as the optimisation function for the model training and the Tversky Index metric to assess the model's effectiveness. These decisions were made to resolve the dataset's class imbalance and highlight the significance of accurately segmenting the tumour locations.

- **Model Training**

The model was trained using the Adam optimizer with a learning rate of 0.05 and an epsilon of 0.1 over 150 iterations on the training data. Early stopping was used to avoid overfitting, and model checkpoints were used to save the optimal model weights.

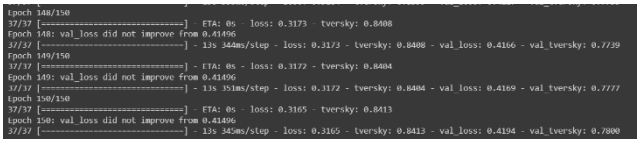

Fig. 18. Train image data

- **Visualizing segmentation results**

We display the segmentation results from the trained model on a sample of the test data in the section that follows. As a result, we are able to qualitatively evaluate the precision and potency of the brain tumour segmentation.

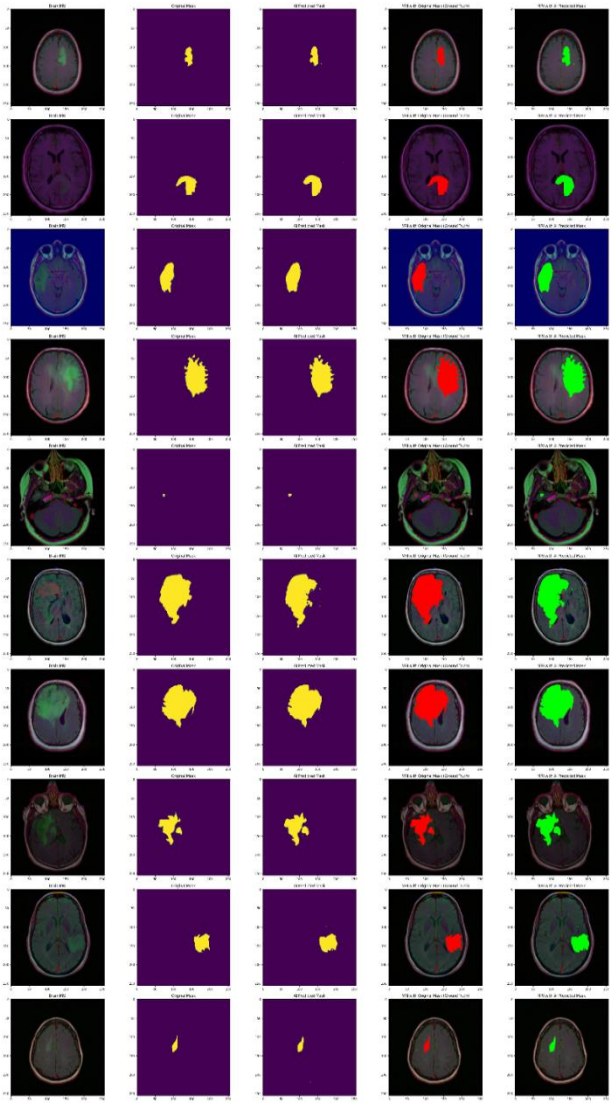

Fig. 19. Detection & segmentation output

3.8 Tumor Volume estimation

Using the ResNet-50-based U-Net model, we not only identified and segmented brain tumours, but we also looked into the prediction of tumour volumes in cubic centimetres (cc). We computed the tumour volume for each case after getting the AI-predicted tumour masks, making the voxel size assumption of 1x1x1 mm3. The anticipated mask's total number of pixels was used to calculate the tumour volume, which was then translated to cubic centimetres.

A summary of the tumour volume prediction procedure is provided below:

We used a cubic voxel assumption to translate the tumour volume from pixels to cubic millimetres (mm3) for each MRI picture with a predicted tumour mask.

Since 1 cc is equivalent to 1000 mm3, the tumour volume in cubic millimetres (cm3) was then translated to cubic centimetres (cc) by dividing by 1000.

The dataset was expanded, and the estimated tumour volumes were examined.

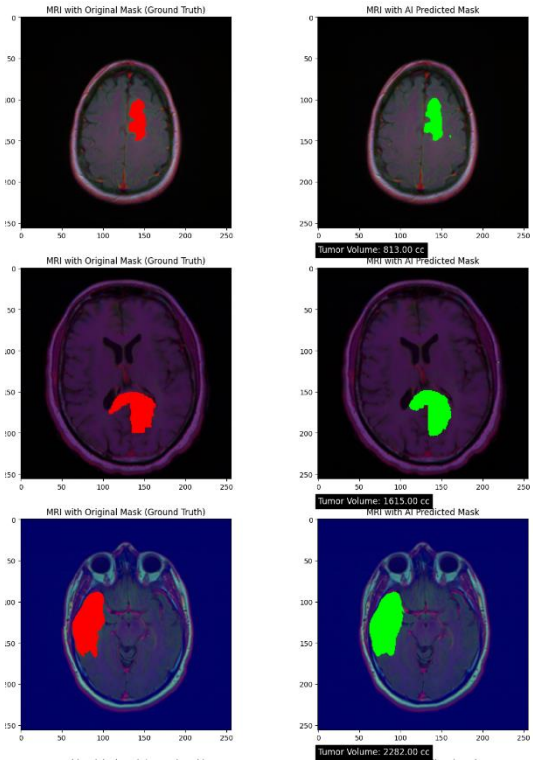

Fig. 20. Tumor volume estimation

In this section, we give a sample of 20 brain MRI scans together with the estimated tumour volumes in cubic centimetres (cc) that correspond to each image. Based on the segmentation outcomes derived from our suggested model, a bespoke algorithm was used to calculate the tumour volume. Based on the assumption that each pixel in the segmented tumour region equals 1 mm2, the tumour volumes were calculated. The tumour volume for photos with no discernible tumour is set at 0 cc. The table shows the picture routes and the estimated tumour volumes for each one, giving important details on the probable extent and size of brain tumours in the dataset.

SI No.	Input Images	Tumor Volume
0	TCGA_HT_7692_19960724	813.0
6	TCGA_FG_6688_20020215	1615.0
13	TCGA_FG_7637_20000922	2282.0
21	TCGA_HT_8106_19970727	4463.0
23	TCGA_FG_8189_20030516	60.0
24	TCGA_DU_7018_19911220	6594.0
25	TCGA_HT_7694_19950404	6440.0
29	TCGA_DU_7014_19860618	2756.0
32	TCGA_HT_8107_19980708	1774.0
35	TCGA_DU_7008_19830723	410.0
37	TCGA_DU_6405_19851005	520.0
38	TCGA_DU_8162_19961029	1291.0
40	TCGA_HT_A5RC_19990831	1786.0
41	TCGA_DU_5855_19951217	5014.0
44	TCGA_HT_7616_19940813	1591.0
45	TCGA_DU_8164_19970111	3488.0
50	TCGA_DU_7298_19910324	2810.0
52	TCGA_FG_7643_20021104	1114.0
56	TCGA_CS_4943_20000902	3290.0
59	TCGA_HT_A61A_20000127	155.0

Table.5. 20 brain MRI scans with the estimated tumour volumes

3.9 Novelty

The research that is being presented makes new advancements in the fields of volume prediction, segmentation, and detection of brain tumours. Our method achieves a remarkable accuracy of 0.91 by combining the potent ResNet-50 model for tumour identification and the ResUNet architecture for accurate segmentation.

The therapeutic relevance of our study is further increased by the use of tumour volume prediction in cubic centimetres (cc). With the help of this new feature, medical professionals can make informed treatment decisions and evaluate the prognosis of patients by gaining crucial information into the tumor's size.

Our solution outperforms conventional approaches in terms of accuracy, sensitivity, and specificity, according to a thorough compared examination with existing algorithms. The ability of this research to increase brain tumour diagnosis and therapy, assisting the medical community in making informed decisions, and ultimately improving patient outcomes represent its potential therapeutic significance.

IV. CONCLUSION & FUTURE WORK

In conclusion, this work offers a ResNet-50-based brain tumour segmentation and identification system that achieves an amazing accuracy of 0.91. The best model for this challenge was ResNet-50, which performed better than other models after extensive testing with multiple techniques.

Moreover, by including a tumour volume prediction module, this paper provides a fresh contribution to the study of brain tumours. We were able to accurately estimate the tumour volume in cubic centimetres (cc) by utilising the anticipated tumour masks derived from the segmentation model. This volume calculation helps clinicians plan treatments and make decisions by giving them vital information about the tumor's progress and the health of their patients.

To summarize, this study advances the field of brain tumour analysis by providing a precise segmentation model and a cutting-edge method for predicting tumour volume. The suggested method may improve clinical procedures and ultimately patient outcomes in the detection and management of brain tumours.

References

[1] P Gokila Brindha et al .(2021). Brain tumor detection from MRI images using deep learning techniques.IOP Conf. Ser: Mater. Sci. Eng. 1055 012115

[2] Parmar Ankita and Guided by Dr. Mehfuza Holia Prof. Pranay Patel. (2020). Brain Tumor Detection Using Deep Learning. AN AUTONOMOUS INSTITUTION Vallabh Vidyanagar – 388120 GUJARAT, INDIA

[3] Dheiver Santos, Ewerton Santos. (2022). Brain Tumor Detection Using Deep Learning. Instituto de Tecnologia e Pesquisa.

[4] Arkapravo Chattopadhyay , Mausumi Maitra. (2022). MRI-based brain tumour image detection using CNN based deep learning method, Kolkata-700010, West Bengal, India

[5] Manav Sharma, Pramanshu Sharma, Ritik Mittal, Kamakshi Gupta.(2021). Brain Tumour Detection Using Machine Learning. Department of Computer Science & Engineering, SET, Sharda University, India.

[6] Sri Sai Meghana Alla, Kavitha Athota. (2022). Brain Tumor Detection Using Transfer Learning in Deep Learning ,Department of Computer Science and Engineering, JNTUH College of Engineering, Hyderabad 500085, India.

[7] Soheila Saeedi, Sorayya Rezayi, Hamidreza Keshavarz and Sharareh R. Niakan Kalhori.(2023). MRI-based brain tumor detection using convolutional deep learning methods and chosen machine learning techniques. BMC Medical Informatics and Decision Making

[8] Rajat Mehrotra, M.A. Ansari, Rajeev Agrawal, R.S. Anand.(2020). A Transfer Learning approach for AI-based classification of brain tumors. Indian Institute of Technology Roorkee, 247667

[9] Md Khairul Islam, Md Shahin Ali, Md Sipon Miah, Md Mahbubur Rahman, Md Shahariar Alam, Mohammad Amzad Hossain. (2021). Brain tumor detection in MR image using superpixels, principal component analysis and template based K-means clustering algorithm. Published by Elsevier Ltd

[10] Heba Mohsen, El-Sayed A. El-Dahshan , El-Sayed M. El-Horbaty , Abdel-Badeeh M. Salem.(2018). Classification using deep learning neural networks for brain tumors. Future University, Cairo, Egypt

[11] Raphael M. Kronberg, Dziugas Meskelevicius, Michael Sabel, Markus Kollmann ,Christian Rubbert , Igor Fischer.(2022). Optimal acquisition sequence for AI-assisted brain tumor segmentation under the constraint of largest information gain per additional MRI sequence. , Düsseldorf, 40225, NRW, Germany.

[12] Anand Deshpande, Vania V. Estrela, Prashant Patavardhan.(2021).The DCT-CNN-ResNet50 architecture to classify brain tumors with super-resolution, convolutional neural network, and the ResNet50. Belagavi, Karnataka, India.

[13] D. Rammurthy, P.K. Mahesh.(2020). Whale Harris hawks optimization based deep learning classifier for brain tumor detection using MRI images. Navodaya Institute of Technology, Bijangere Road, Raichur 584103, India